JOURNAL OF MATERIALS SCIENCE **36** (2001) 3607–3615

# Comparison of microstructure and solidification behavior of rapid quenching with bulk undercooled superalloy

FENG LIU*, GENCANG YANG, XUEFENG GUO
*State Key Laboratory of Solidification Processing, Northwestern Polytechnical University, Xi'an Shaanxi, 710072, People's Republic of China*
*E-mail: caoyang77@263.net*

Microstructure and solidification behavior in rapid quenching (i.e., gas-atomized powders and melt-spun ribbons) of superalloy have been compared with bulk undercooled superalloy. The application of a molten salt denucleating technique combined with thermal cycle enables such investigation over a wide range of undercooling up to 210 K. The microstructure formation has been discussed for both methods of solidification with respect to undercooling, nucleation, and recalescence as well as recrystallization during post-recalescence. Comparison of the observed microstructure and morphologies indicates that the melt-spun ribbons and the gas-atomized powders with cooling rate above $10^4$ K $sec^{-1}$ crystallize only after achieving a large degree of undercooling, which becomes higher and higher with the increase of cooling rate. Furthermore, it should be noted that, grain refinements, which play a decisive role in the undercooled as-solidified structure, however, result from different sources in the rapid quenching process.


## 1. Introduction

Nowadays, rapid solidification (RS) has become an important technique for producing novel alloys of metallic, intermetallic and ceramic materials. Laser surface treatment, melt atomization and melt spinning, as well as planar flow castings are the main representatives of modern RS-processes [1]. The understanding of microstructure formation under the RS-conditions has therefore become a major issue in solidification theory. With the advent of rapid solidification technologies, ultra-rapid quenching (e.g. melt-atomization or melt spinning) has become a subject of considerable interest in the development of aircraft structure and engines. For the control of solidification with respect to grain refinement or microsegregation-free crystallization, it is necessary to understand how the rapid quenched microstructure evolves, and how it depends on processing conditions. In this respect, the department of Materials science of ONERA [2] launched a research program on rapid quenching of superalloy. The first objective is to asses the possible benefit that could arise from rapid quenching of nickel-base superalloy and its possible application to disc and turbine blades.

Nevertheless, the direct application of rapid quenching processing is applicable only in such small volume components as gas-atomized powders or melt-spun ribbons, bot not suitable for the preparation of three-dimensional bulk products. The rapid solidification processing of highly bulk undercooled melt is of a notable advantage that it is not restricted by the sample size [3]. Three-dimensional bulk amorphous [4], metastable [5] and refined microstructure [6] can be obtained by adopting this technique. With slowly cooled bulk undercooled samples, the rapid crystallization of undercooled melts and the influence of undercooling on the resulting microstructures can be studied independent of external high-speed parameters. In melt spinning of crystalline ribbons and gas atomized powders, generally only a cooling rate is regarded as responsible for microstructure formation. However, little attention has up to now been paid to the degree of superalloy melt undercooling prior to solidification and its influence on growth rates and mechanism. Therefore, the difference and the similarity in rapid solidification behavior and microstructure formation between rapid quenching and bulk undercooled superalloy melts deserve thorough discussion.

The employment of molten salt covering, denucleating and high frequency induction heating under the protection of argon atmosphere enables substantial undercooling of superalloy melt in the non-catalytic coating mold [7]. The possibility of determination and control of sample temperature allows a correlation between

* Author to whom all correspondence should be addressed.

TABLE I Nominal composition of the DD3 single crystal superalloy [10]

| Element | Cr | Al | Ti | W | Co | Mo | Ni |
|---|---|---|---|---|---|---|---|
| Wt% | 9.5 | 5.9 | 2.2 | 5.2 | 5 | 3.8 | balance |

undercooling and evolution of microstructures. The paper presents the results of preliminary work carried out in the state key laboratory of solidification processing at Northwestern Polytechnical University (N. P. U.) [8]. The aim of this work is to compare the solidification behavior and microstructure of gas-atomized and melt-spun superalloy [4] with the slowly undercooled samples.

## 2. Experimental procedure

Commercial DD3 single crystal superalloy (Table I) was chosen in the bulk undercooling experiment, which was established by the application of molten salt covering, denucleating and high frequency induction heating under the protection of argon atmosphere. Prior to melting, the surfaces of the metal charges were cleaned mechanically by grinding off the surface oxide layer and chemically by etching in HCl solution diluted by alcohol. When beginning experiment, the alloy charges were placed in a cleaned and dried non-catalytic coating mold [7], and covered with a 5 mm layer of salt granules. Then the mold was sealed, evacuated and subsequently back-filled with 99.999% argon gas. Each sample was melted, superheated, solidified and subsequently remelted in superheating-cooling cycles, aming at obtaining large undercoolings. Here, this non-catalytic coating mold is a kind of shell mold (composed of 79 $SiO_2$, 18 $ZrO_2$, and 3 $B_2O_3$, wt%), over whose inner surface a glass coating with the same composition is deposited. It was found in the experiment that, this coating mold can keep amorphous or less-crystalline at high temperature for a long time, and consequently, prevent premature nucleation of superalloy melt in contact with it, indicating an ideal non-catalytic nucleation inhibition for DD3 single crystal superalloy [7]. After experiment, the composition analysis, performed in the inner surface of coating mold and alloy samples achieved, clarified that no chemical reaction occurred between the alloy melt and the mold materials and the salt granules. So the composition of the resultant as-solidified specimens was taken to be the same as the original composition. The thermal behavior of samples was monitored by an infrared pyrometer with an absolute accuracy, relative accuracy, and response time of less than 10 K, 3 K, and 5 ms, respectively [9]. The cooling curve was calibrated with a standard PtRh30-PtRh6 thermal couple, which was encapsulated in a tube composed of the same material as the non-catalytic coating mold and then immersed into the melt in the identical condition. The melting temperature and the undercooling of the alloy in the cooling curves could be read after the comparison with the absolute temperature recorded by the standard thermal couple.

Each of the samples had a weight of 10–15 g and a diameter of 8–12 mm, and was sectioned through the triggering spot, then polished, and etched with an aqueous solution of $FeCl_3$ and HCl. Structure observation was carried out with optical microscope, scanning electron microscopy (SEM) and transmission electron microscopy (TEM), respectively.

## 3. Experimental results

### 3.1. Solidification microstructures in gas-atomized powders and melt-spun ribbons of Stellite 6 superalloy

Examination of polished and etched sections of embedded Stellite 6 powders by SEM [2] showed that essentially three distinct types of solidification microstructures were presented in classical gas-atomized powders corresponding to various particle diameters. The finer particles with diameters less than 50 $\mu$m, exhibited a typical dendritic pattern, whereas the coarse fraction of the atomization product (above 100 $\mu$m diameter) presented an equiaxed microstructure. In addition, a substantial fraction of the powders, less than 20 $\mu$m diameter, exhibited a completely different type of structure that appeared to be cellular or microcrystalline, depending largely on quenching conditions.

Furthermore, the typical solidification microstructure observed in a 30 $\mu$m thick melt-spun ribbon clearly exhibited three distinct zones [2]: (1) a fairly featureless chill zone about 4–5 $\mu$m thick; (2) a columnar dendritic region usually extending across the major part of the ribbon thickness (20 $\mu$m); (3) a randomly oriented dendritic region 3 to 4 $\mu$m thick extending to the top surface of the ribbon.

### 3.2. Undercooled solidification structure of DD3 superalloy

Here, high undercooling up to 210 K has been achieved in DD3 single crystal superalloy melt. The grain size and typical microstructure at various undercooling are shown in Figs 1, 2, and 3 respectively. The characteristic undercooling $\Delta T_1$, $\Delta T_2$, $\Delta T_3$, $\Delta T_4$, $\Delta T_5$ and $\Delta T^*$

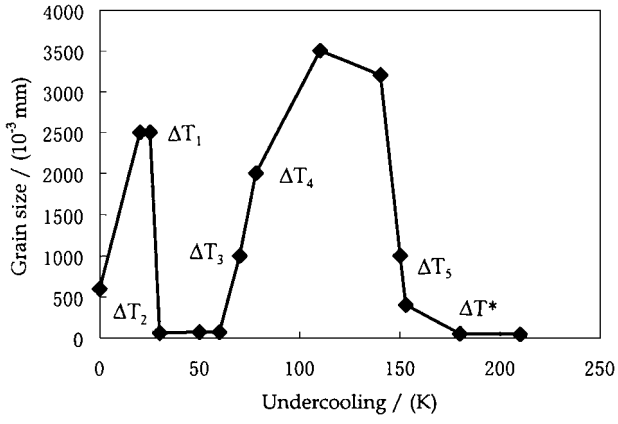


*Figure 1* Variation of the grain size of DD3 single crystal superalloy with undercooling.

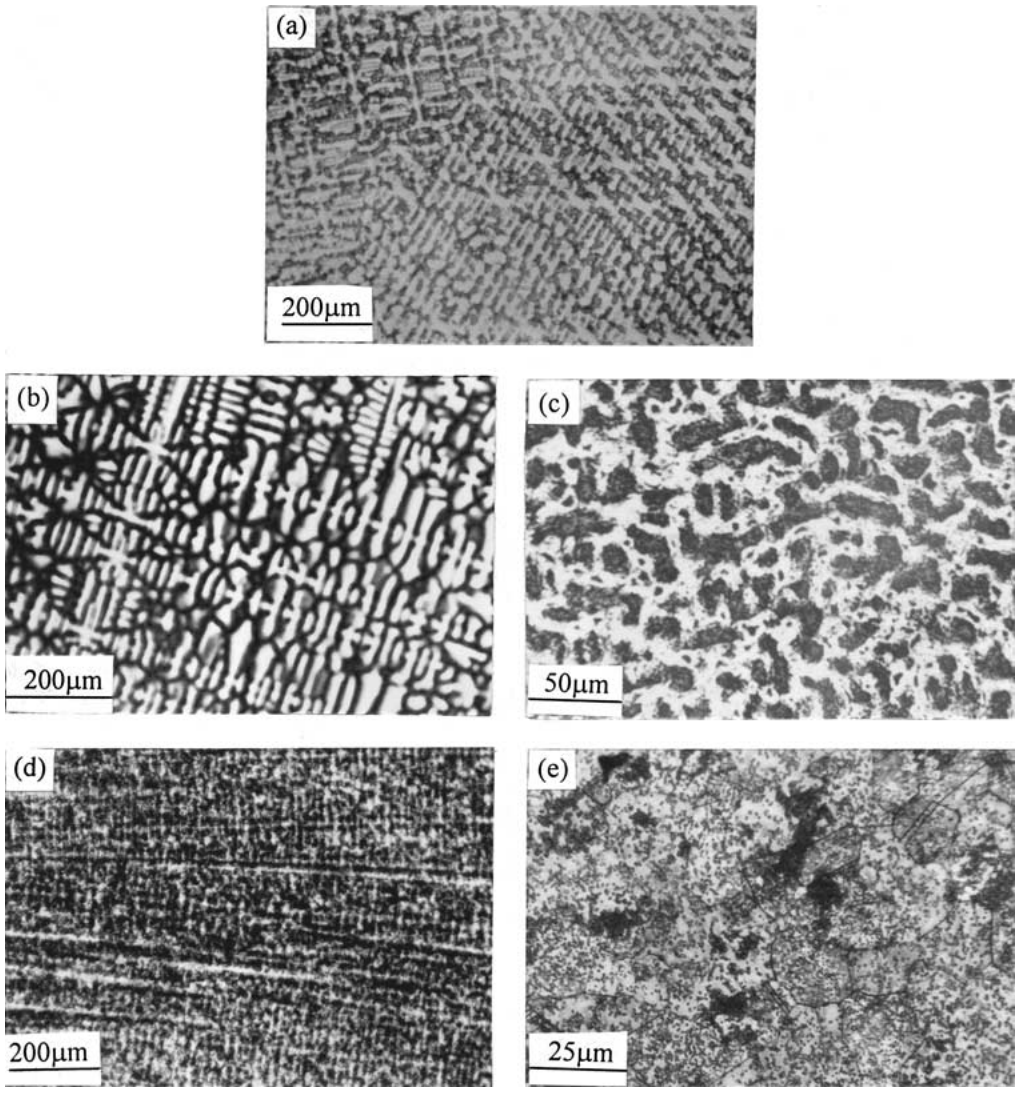


*Figure 2* Microstructure evolution of DD3 single crystal superalloy at undercoolings of (a) 0 K, (b) 25 K, (c) 45 K, (d) 130 K, (e) 200 K.

is 25, 30, 70, 78, 150 and 180 K, respectively. Within the achieved range of undercooling 0–210 K, solidification structure with undercooling could be classified as four categories. A typical branched dendritic structure is seen in the case of non-undercooled sample (Fig. 2a). Then introducing a small undercooling into the alloy promotes the formation of highly branched dendrite (Fig. 2b) and enlarges the grain size (Fig. 1). When $\Delta T > \Delta T_1$, a substantial ripening of the dendrites comes into being. For the sample nucleated at $\Delta T_2$–$\Delta T_3$, the overall cross-section is occupied by refined grains with a diameter of 50–70 $\mu$m (see Figs 1, 2c and 3a), and then a further increase of undercooling leads to the rise of grain size again (Fig. 1). $\Delta T_4$ is defined as the characteristic undercooling from which there are no obvious dendritic fragments in the structure, and only several large crystals are found. During $\Delta T_4$–$\Delta T_5$, the microstructure consists of the developed fine dendrite (Fig. 2d). From $\Delta T_5$, the grain size decreases abruptly (Fig. 1). When $\Delta T > \Delta T^*$, the overall structure is refined again, the aforementioned dendritic structure is fully substituted by equiaxed crystals with average grain size less than 50 $\mu$m (Figs 2e and 3b), in which many twins are found (Fig. 2e).

## 4. Discussion

### 4.1. Various solidification microstructures of DD3 single crystal superalloy with respect to different undercooling range

#### *4.1.1. Solidification characterization of the DD3 single crystal superalloy*

The constituents of DD3 single crystal superalloy, shown in Table I, have been classified as solid solution and/or precipitate formers. Two phases, matrix and strengthening phase predominantly exist in the as-cast structure. It is also shown in reference [11] that the Ni-Cr-Al-Mo system is of particular interest in representing the equilibria among $\gamma$ (nickel-rich solid solution), $\gamma'$ (based on $Ni_3Al$) and $\sigma$ phases, and that the Ni-Cr-Al-Mo systems consist of single $\gamma$−Ni (Al, Cr, Mo) phase above 800°C, if having the same Al, Cr, Mo content as that in DD3 single crystal superalloy, respectively. Furthermore, Machlin and Shao [12] have proposed the extension of the Ni-Cr-Al-Mo quaternary to higher order alloys by adopting the scheme of equivalents (Ni, Co, Fe) : Cr : (Al, Ti) : (Mo, W, Nb, V, Ta, Hf). It then follows that similarity exists in the solidification characterization between the Ni-Cr-Al-Mo system and DD3 single crystal superalloy, which can solidify as single $\gamma$ phase in the rapid

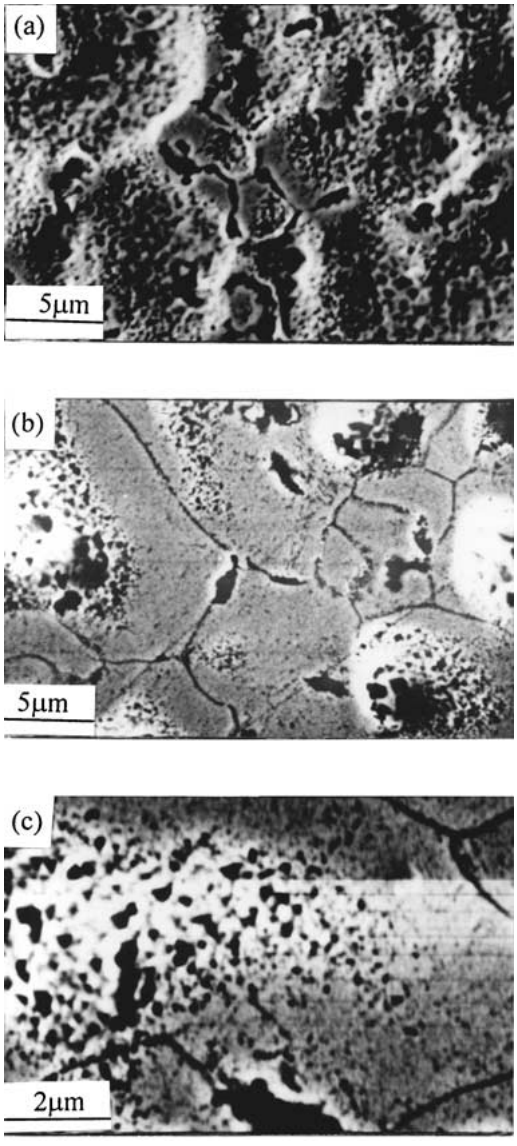


*Figure 3* The morphologies of the refined structures of DD3 single crystal superalloy (SEM): (a) $\Delta T = 50$ K, (b) $\Delta T = 180$ K, and (c) $\Delta T = 210$ K.

dendritic solidification process. The solidification process of undercooled DD3 single crystal superalloy is as follows. First, dendrites, are formed at the nucleation point and grow rapidly through the mass of the melt. They consist of $\gamma$ phase (Ni alloyed with Al, Ti, W, Mo, Co, Cr) [10]. Then the rapid release of heat of fusion during dendrite growth results in rapid recalescence, with possible remelting of the dendrite network. Finally, the remaining interdendritic liquid starts to solidify onto the dendritic network at low melt undercooling in post-recalescence. During the relatively long duration of this final stage, diffusional coarsening occurs, and $\gamma/\gamma'$ eutectic (1 volume pct in the cross-section of the sample) is formed between $\gamma$ dendrites [13]. During subsequent cooling, $\gamma'$ precipitates within the $\gamma$ phase [14]. Without considering the effects of element Ti, W, Co on the solidification behavior, the physical parameters of the Ni-Cr-Al-Mo (9.5%Cr, 5.9%Al, 3.8%Mo, wt%) $\gamma$ phase, listed in Table II, are rendered as the approximant of the DD3 single crystal superalloy.

TABLE II The physical parameters of $\Upsilon$ solid solution [15, 16]

| Parameter | Symbol | Units | Values |
|---|---|---|---|
| Heat of fusion | $\Delta H_f$ | KJ mol$^{-1}$ | 16 |
| Specific heat | $C_P^l$ | J K$^{-1}$ mol$^{-1}$ | 40 |
| Slope of liquidus | $m$ | K (at%)$^{-1}$ | $-4.1$ |
| Partition coefficient | $k_0$ | | 0.81 |
| Diffusion coefficient | $D$ | m$^2$ s$^{-1}$ | $6 \times 10^{-9}$ |
| Thermal diffusivity | $\alpha$ | m$^2$ s$^{-1}$ | $6 \times 10^{-6}$ |
| Atomic spacing | $a_0$ | m | $3.2 \times 10^{-10}$ |
| Sound speed in liquid alloy | $V_0$ | m $\cdot$ s$^{-1}$ | 2000 |
| Interfacial energy | $\sigma$ | J m$^2$ | 0.43 |

### 4.1.2. The dendrite growth in the undercooled DD3 single crystal superalloy melt

The crystal growth in the undercooled melt is influenced not only by thermal diffusion, solute diffusion and liquid/solid interface tension, but also by the interfacial attachment kinetics which becomes more and more significant as the undercooling increases. As mentioned above, except for the constraint of the mold wall, there are no other external factors imposed on the dendritic solidification, so the dendrite growth can still be described by the theory of free dendrite growth. According to BCT model [17], the total undercooling at the dendrite tip consists of four contributions.

$$\Delta T = \Delta T_t + \Delta T_c + \Delta T_r + \Delta T_k \tag{1}$$

where $\Delta T_t$, $\Delta T_c$, $\Delta T_r$, and $\Delta T_k$ are the thermal undercooling, solute undercooling, curvature undercooling and interfacial kinetic undercooling respectively. The expression for each kind of undercooling can be found in Ref. [17]. In addition, the solute concentration of the liquid at the dendrite tip $C_L^*$, can be written as:

$$C_L^* = \frac{C_0}{1 - (1-k) I_V(P_C)} \tag{2}$$

where $C_0$ is the nominal composition of the alloy, $I_V(P_C)$ is the Ivantsov function of the solute Peclet number $P_C$, and $k$ is the growth velocity dependent non-equilibrium solute partition coefficient that can be used to evaluate the lever of solute trapping [18], a model describing the transition between solute equilibrium and partition-less solidification, developed by Aziz.

$$k = \frac{k_0 + V/V_D}{1 + V/V_D} \tag{3}$$

where $V_D = D/a_0$ is the solutal diffusion speed, $V$ is the advancing velocity of solid/liquid interface, and $k_0$, $D$, as well as $a_0$ are the equilibrium solute partition coefficient, the solute diffusivity, and the characteristic length of solutal diffusion in the liquid alloy, respectively. Using the foregoing equations and the physical parameters of the DD3 single crystal superalloy [10] listed in Table II, the undercooling contributions at different initial undercooling, the crystal growth velocity, and the solute concentration of the liquid at the growing

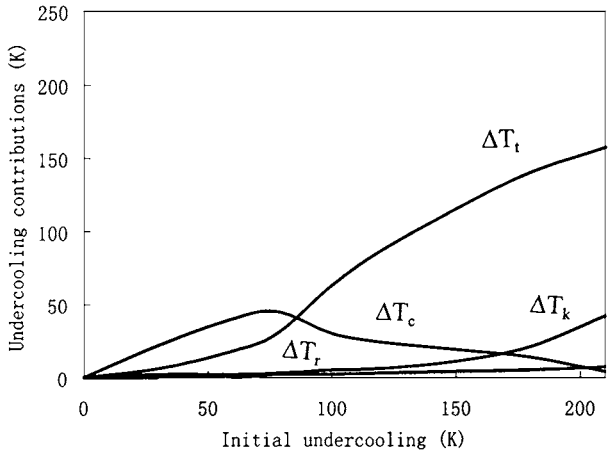


*Figure 4* Undercooling contributions at the dendrite tip vs. initial undercooling of the DD3 single crystal superalloy.

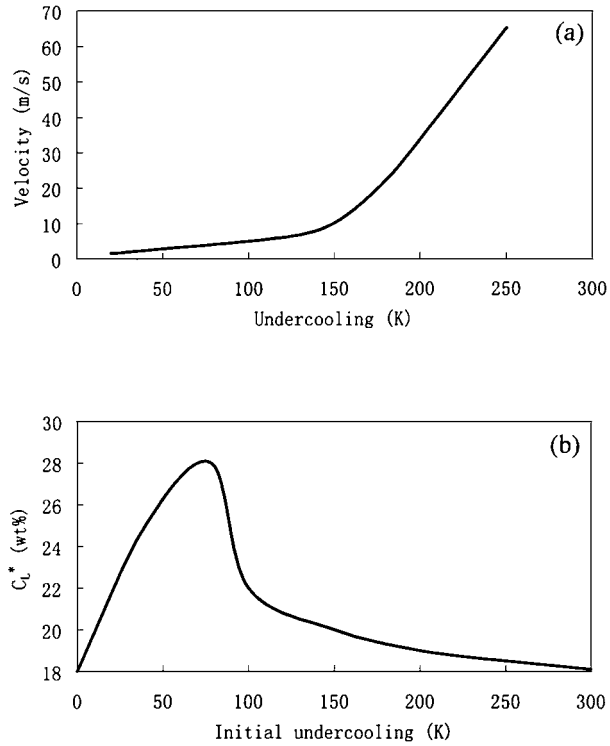


*Figure 5* Dendrite growth velocity (a) and concentration of solute in liquid (b), at the dendrite tip vs. initial undercooling of DD3 single crystal superalloy.

dendrite tip can be calculated. The results are illustrated in Figs 4 and 5. It is well known that [19], in single-phase alloys, the condition of diffusional equilibrium is gradually becoming less important with the increasing of solidification velocity and undercooling in front of the dendrite tip. Therefore, solute rejection is reduced and solutal undercooling decreases as the interface concentration approaches the melt composition. This ultimately causes partition-less solidification, which is solely controlled by thermal gradient. Here, for undercooling range less than $\Delta T_2$, the solutal undercooling is much greater than the thermal undercooling, and the dendrite growth is dominantly controlled by the solutal diffusion (Fig. 4). As the undercooling continuously increases, the effect of thermal diffusion on the dendrite growth becomes strong. When $\Delta T > \Delta T_4$, the thermal undercooling is higher than the solutal undercooling in front of the dendrite tip (Fig. 4). Solute diffusion is replaced by the thermal diffusion to predominantly control the dendrite growth process, which indicates a transition from the equilibrium of a solidification controlled by the solutal gradient to a thermally controlled growth owing to a relaxation of diffusional equilibrium at the solid-liquid interface. Therefore, the higher the undercooling and the thermal undercooling, the more convenient for dissipating of the latent heat of dendrite tip in the crystal growth. Once nucleus forms from the undercooled melt, dendrite will radially and rapidly grow into the undercooled liquid. When the growth velocity becomes large enough to make k obviously deviate from $k_0$ (see Fig. 5a), the convergence of the growth velocity dependent non-equilibrium liquidus and solidus [18] as well as the decrease of $C_L^*$ and $\Delta T_c$ (see Figs 5b and 4), are bound to take place. This infers that the essential prerequisite for dendrite ripening is not provided.

Furthermore, It was also shown in Ref [20], that the dimensionless superheating of the central part of the dendrites stems (i.e. the initially frozen solid) in the recalescence can be used to evaluate the dendrite remelting. Then,

$$\Delta \bar{T}_S' = \frac{T_R - T_S'}{\Delta T_0'} \tag{4}$$

where, $\Delta \bar{T}_S'$ is the dimensionless superheating, $T_R$ the highest recalescence temperature corresponding to $\Delta T$, $\Delta T_S'$ the equilibrium solidus temperature with respect to the composition $C_S'$ of the central part in the dendrite stem, and $\Delta T_0'$ the equilibrium crystallization temperature range of the alloy with $C_S'$. It is known,

$$T_S' = T_L + m\left(\frac{C_S'}{k_0} - C_0\right) \tag{5}$$

$$\Delta T_0' = mC_S'\left(1 - \frac{1}{k_0}\right) \tag{6}$$

where $T_L$ is the equilibrium liquidus temperature of the alloy with initial composition $C_0$, and $m$ the equilibrium liquidus slope. From the steady diffusion solution at the dendrite tip, $C_S'$, the solid composition at the dendrite tip can be expressed as:

$$C_S' = \frac{kC_0}{1 - (1-k)I_V(P_c)} \tag{7}$$

Employing the method described in Ref 21 according to the laws of conservation of energy and mass, we can calculate $T_R$, provided that the solidification during the recalescence occurs under the adiabatic condition and that the specific heats of the solid and liquid are constant and equal. Finally, the relationship between dimensionless superheating $\Delta T_S'$ and undercooling $\Delta T$ of DD3 superalloy is obtained and presented in Fig. 6. Obviously, with increasing undercooling, $\Delta T_S'$ first rises up to its maximum and then descends. The dimensionless superheatings in the rapid recalescence of the samples undercooled by $\Delta T_4$–$\Delta T_5$ (see Fig. 6) is located in the

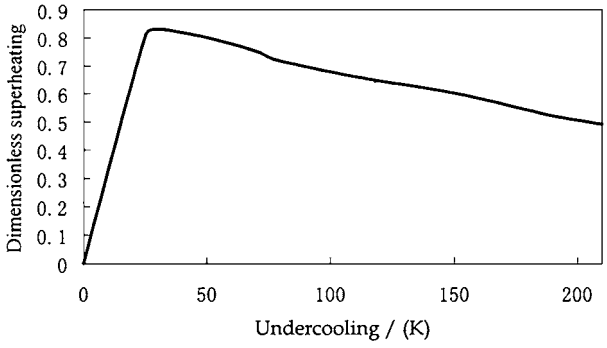


*Figure 6* Dimensionless superheating of DD3 single crystal superalloy vs. initial undercooling.

low temperature range, i.e. the essential thermal prerequisite for dendrite ripening is not guaranteed in this undercooling range. Therefore, compared with that undercooled by $\Delta T_2$–$\Delta T_3$, the fraction of dendrite remelting in recalescence is relatively low, which results in the formation of directional solidified structure, as shown in Fig. 2d.

### 4.1.3. Mechanism of the grain refinements

A new analytic model that describes solidification of equiaxed dendrites was presented by L. Nastac, and was used to simulate the solidification of INCONEL 718 superalloy casting [22]. The predications generated with this model are shown to agree very well with experiments. Meanwhile, various models have been proposed to predict equiaxed grain density [23], diffusional process [24], and phase formation [25] in the superalloy melt. Nevertheless, these models are all based on the same assumption: small undercooling and low growth velocity, which is not favor of the investigation in grain refinements here. In present paper, however, different physical origin plays a dominant role in grain refinements with the rising of undercooling. At the undercooling range of $\Delta T_2$–$\Delta T_3$, dendrite growth is dominantly controlled by the solutal diffusion, so $C_L^*$ and $\Delta T_c$ increase obviously with increasing undercooling, which is in agreement with the results of BCT model calculation shown in Figs 4 and 5. Moreover, it is found that all of the maximum dimensionless superheating (Fig. 6) are located in this undercooling range, which provides remaining liquid a relatively higher temperature and longer solidification time during post-recalescence. Therefore, combined with the results obtained from Figs 2c and 3a, it can be concluded that the dendrites solidified in the undercooling range of $\Delta T_2$–$\Delta T_3$ have the maximum tendency to be remelted and ripened in recalescence and subsequent post-recalescence, respectively. The first refinement is therefore attributed to the dendrite break-up or ripening owing to remelting.

When the undercooling is beyond $\Delta T_5$, contrarily, the dimensionless superheating of the dendrite decreases to the lower temperature range (Fig. 6), consequently, the remelting is not severe enough to make the dendrite disintegrate into fine granule. The grain refinement at high undercooling must be induced by other factors rather than remelting. A physical mechanism has been proposed, that the break-up of dendrites under the action of remelting causes the grain refinement at the critical undercoolings, and it occurs when the thermal plateau time during solidification $t_{pl}$ exceeds the time for break-up by Rayleigh instability $t_{bu}$ [26]. However, this model uniquely considers the break-up driven by the liquid/solid interface tension, ignoring the action of high stress produced in the rapid solidification, whereas the latter may play a more important role in the dendrite break-up. In connection with the microstructure shown in Figs 2, 3, the average grain diameter is not comparable with the side-branch spacing, yet is several times larger than the spacing. The grain boundaries, which evolve from curve-line to straight-line and intersect each other to form annealing hexagons (Fig. 3b and c), become much narrower than that originates from the solidification segregation in the lower undercooling range (Fig. 3b). Fig. 3c also shows that dendrite substructure appears in this kind of grain. Therefore, we suggest that the grain refinement at the critical undercooling should result from the recrystallization process as argued by Powell *et al*. [27, 38], which appears to occur during, or immediately after, solidification, while the solid metal is very close to the melting point. The occurrence of recrystallization requires a driving force, which is provided, under normal condition, by prior plastic deformation. In the present case, however, it is the high stresses produced during the extremely rapid solidification process, but not any external agency, that result in the dendrite distortion and fragment or plastic deformation, and finally, recrystallization as well.

If the dendrite growth is too great to permit complete diffusion of solute out of the melt in contact with the advancing tip, effective solute trapping may occur in the solid [18]. As a result of high-velocity growth after large undercooling (beyond $\Delta T^*$), a high energy content of the first-formed structure also can be expected to be built in, in the form of a high population of crystalline defects, such as dislocations and grain boundaries (Fig. 7). The higher the undercooling, the more the defects. Also, it should be noted that the center of mass of an undercooled melt should undergo a substantial acceleration during freezing due to the rapid change from liquid to solid density at the very high freezing rates involved [28]. Therefore, the first-formed dendrite would be subject to fracture, disintegration owing to high stress arising from this kind of rapid heterogeneous shrinkage process, which results in the recrystallization structure shown in Figs 2e and 3c.

## 4.2. Relationship between undercooling and cooling conditions in gas atomization and melt spinning

In order to obtain a better understanding of the heat flow and solidification behavior of convectively cooled droplet, cooling conditions in melt-atomization were studied using the solidification time, $t_s$, as the determining parameter. For this purpose, $t_s$ was evaluated in two ways [2]. Firstly, a simple estimation of $t_s$ was made from the quenching rates, $T^*$, using the relationship

TABLE III Calculated and measured $t_s$, cooling rate and corresponding degree of undercooling vs. various particles size in atomization and melt spinning

| Particle diameter ($\mu$m) | Cooling rate $T^*$ (K sec$^{-1}$) | $t_s$ (measured) ($\mu$sec) | $t_s$ (calculated) ($\mu$sec) | Undercooling (K) |
|---|---|---|---|---|
| 400 | $9 \times 10^2$ | $7.78 \times 10^4$ | $7.78 \times 10^4$ | 0 |
| 200 | $3.4 \times 10^3$ | $2.06 \times 10^4$ | $2.06 \times 10^4$ | 0 |
| 100 | $1.4 \times 10^4$ | $5 \times 10^3$ | $5 \times 10^3$ | 0 |
| 50 | $5 \times 10^4$ | 1400 | 1600 | 53 |
| 20 | $2.8 \times 10^5$ | 250 | 400 | 158 |
| 10 | $1.1 \times 10^6$ | 63.6 | 130 | 207 |
| Melt spun ribbon | $>10^7$ | <10 | <15 | >450 |

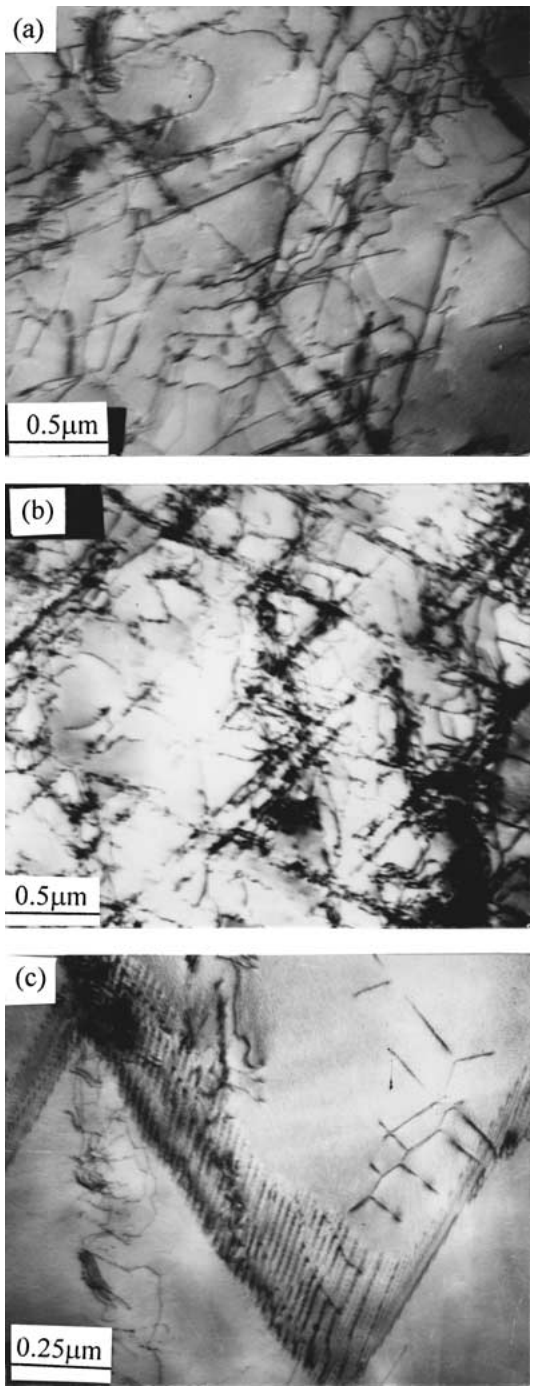


*Figure 7* Formation of dislocation tangle (a), dislocation deformation cell (b), and sub-boundary constructed by dislocation (c) in the as-solidified undercooled superalloy (TEM): (a) $\Delta T = 170$ K, (b), (c) $\Delta T = 210$ K.

$t_s = \Delta T / T^*$, where $\Delta T$ is the freezing range of the alloy [29]. Secondly, $t_s$ was calculated by using a simple relationship valid in the case of Newtonian cooling regime. The assumption of Newtonian cooling is supported by the fact that, in the case of convectively cooled droplets ranging from 100 to 400 $\mu$m, the Biot number remains below 0.1 [30]. Under these conditions, the solidification time can be simply derived as follows:

$$t_s = \frac{(R\rho H \Delta T)}{[3h(T - T_0)]} \tag{8}$$

where, $R$ is the radius of the droplet, $T_0$ the temperature of the atomizing gas, $H$ the heat of fusion, $\rho$ the density of the alloy, and $h$ the heat transfer coefficient. In order to facilitate the discussion below, the cooling rate, the calculated $t_s$, measured $t_s$ and the corresponding undercooling versus different particle size during gas-atomization and melt spinning, are reproduced in Table III from Ref. 4. It is found that, the calculated $t_s$, for particles larger than 100 $\mu$m diameter, is equal to the measured ones, which indicate that Equation 8 is suitable for the calculation of $t_s$ in this particle range, i.e., in this cooling rate range. For particle size smaller than 100 $\mu$m, however, the measured $t_s$ is much smaller than the calculated ones, which clarifies that the high quench rates achieved in finer particles can not be explained by the same way as that in particles larger than 100 $\mu$m diameter. This phenomenon suggests that convective radiative cooling alone could not explain the high solidification rate achieved in the finer particles (<100 $\mu$m). The sole phenomena that can account for measured solidification times smaller than the calculated ones must be undercooling of the melt.

Solidification time is directly proportional to the latent heat of fusion ($H$). If a droplet is undercooled from the melting point ($T_m$) to the nucleation temperature ($T_n$), the amount of heat to remove by convective cooling to complete solidification will be reduced to $H - C_p(T_m - T_n)$, where $C_p$ is the mean specific heat of the solid and liquid. Similarly, the solidification time of an undercooled droplet is therefore reduced by a factor

$$R = 1 - C_P / H(T_m - T_n) \tag{9}$$

So we can concluded that, (a) quench rates ranging from $10^2$ to $10^4$ K sec$^{-1}$ in powder particles of 400 to 100 $\mu$m diameter could be achieved by cooling alone,

respectively. (b) It is from a high undercooling that high quenching rates experienced by the smaller particles essentially result, typically 200 K for 10 $\mu$m diameter particles. Also, the entire melt-spun ribbon, as shown in Table III, is cast at quench-rates exceeding that in atomization, indicating that undercooling plays a more important role in melt-spinning than in atomization.

### 4.3. Comparison of microstructures and solidification behavior in rapidly-quenched and bulk undercooled superalloy

In present work, different microstructures, as analyzed above, are formed according to various undercooling obtained, and can be concluded as follows. When $\Delta T < \Delta T_3$, the refined equiaxed structure, attributed to the dendrite break up or ripening owing to remelting, corresponds to that in the gas-atomized particles with diameter above 100 $\mu$m and that in the top surface of melt-spun ribbon. When $\Delta T_4 < \Delta T < \Delta T_5$, the fine dendritic structure caused by heterogeneous nucleation in highly undercooled melt, is equivalent to that achieved in atomization product (less than 50 $\mu$m diameter) and that achieved across the major part of the ribbon thickness. When undercooling is beyond the critical value ($\Delta T^* = 180$ K), quasi-spherical crystal is formed as a result of the second grain refinement, which stands for the occurrence of massive transformation. This phenomenon is also proved by the appearance of microcrystalline in atomization particles less than 20 $\mu$m diameter. However, the featureless structure in the microsegregation-free chill zone achieved in melt-spun ribbons can not be obtained here. Since the minimum undercooling required to complete solidification without segregation can be easily estimated as suggested by Mehrabian [29],

$$C_P[(T_L - T_n) + (T_s - T_L)] \geq H \qquad (10)$$

where, $T_L$ is the liquidus temperature, $T_s$ the solidius temperature, $T_n$ the nucleation temperature. Therefore, the undercooling ($T_m - T_n$), according to Equation 9, must exceed 450 K in Nickel-base superalloys. In fact, the quench rates attained in atomization powders, even in the ultrafine size range, are not sufficient to achieve the high degree of undercooling required for complete massive transformation. Melt spinning is supposed to achieve degree of undercooling so far not available by any bulk undercooling experiment. As a result, the above consideration clearly demonstrates that the degree of undercooling required to produce fully microcrystalline i.e., the complete massive transformation, can not be attained by gas-atomization and bulk undercooled rapid solidification.

Compared with that occurring in the bulk undercooled solidification, however, grain refinements in rapid quenching have different sources. In bulk undercooled solidification, recalescence plays an important role in controlling the as-solidified structure. The total amount of enthalpy in the crystallization process and the heat capacity of the system set an upper limit to the temperature of sample during recalescence. The temperature is, of course, a crucial parameter for the action of secondary process such as structural transformation, compositional partitioning, coarsening or even remelting, and such has an important influence on the morphology of the final product [31]. The first grain refinement result from the dendrite break-up or ripening owing to remelting in recalescence. The second refinement is attributed to the stress that originates from the extremely rapid solidification process, which result in the dendrite distortion, disintegration and recrystallization during post-recalescence. The undercooled solidification is essentially adiabatic during rapid recalescence. This is confirmed by estimate of the ratio of the dimensionless kinetic coefficient to the Biot number [32]. This ratio, which is a measure of the predominance of the recalescence rate over the rate of heat loss to the environment, is calculated to range from $10^3$ to $10^5$. In rapid quenching process with cooling rate above $10^4$ K $sec^{-1}$, however, this ratio is much less than that in bulk undercooled solidification, which indicates that the so-called recalescence in rapid quenching is not obvious, and can not influence the as-solidified structure effectively.

During the atomization process [2], droplets of different diameters experience varying cooling rates and require various time to complete solidification process, i.e. the larger the diameter is, the longer the predendrites stays in solid/liquid mesh zone. Thus, the equiaxed structure can be interpreted as the consequence of nucleation on fragments of predendrites. These fragments of predendrites may result from partial dissolution of predendrites in a way similar to that produced by a processing technique known as stir-casting in which semi-solid material containing predendrites is highly sheared during cooling through the melting-range [2]. It should be called dynamic refinement. The dendritic structure results from heterogeneous nucleation occurring in highly undercooled droplets. The microcrystalline structure is formed by a massive transformation resulting from homogeneous nucleation at a high degree of undercooling. But it was not possible to detect fully microcrystalline particles in atomization powders as a result of the insufficient undercooling before nucleation. A detailed investigation of the microstructure of melt-spun superalloy ribbons revealed that the cooling rate achieved in the immediate vicinity of the chill substrate was much higher than that achieved in atomization powders. Consequently, liquid alloy in the immediate vicinity of the chill can achieve a very high undercooling, and then, solidify fast enough to obtain a fairly featureless chill zone i.e., microcrystalline structure. The transition from a dendritic to a microcrystalline structure in melt-spun ribbons can be related to the corresponding transition in bulk undercooled sample at the critical undercooling.

In both bulk undercooled solidification and rapid quenching process, however, thermal gradient is a decisive factor in controlling the as-solidified structure. As illustrated in rapid quenching with cooling rate above $10^4$ K $sec^{-1}$ (Table III), the non-Newtonian cooling is a predominant process that controls the melt solidification. The heat transport from the molten layer to the

solid part is the main controlling mechanism. The temperature gradient across the molten layer is the characteristic parameter of the solidification process. The temperature gradient induces a non-equilibrium state and the decreasing of it leads to the crystallization. Similarly, it is the thermal diffusion controlled by thermal gradient, in bulk undercooled solidification, that becomes more and more effective and determines the final structure and morphology.

## 5. Conclusion

The aim of this paper is to compare microstructure of rapid quenched (gas-atomized and melt-spun) superlloy with slowly bulk undercooled samples in order to estimate the lever of melt undercooling in the rapid quenched products prior to crystallization as well as the relationship between cooling rate and undercooling achieved.

1. Comparing the microstructure of gas-atomized particles (e.g., the microstructure of samples with diameter less than 20 $\mu$m, 50 $\mu$m and above 100 $\mu$m, respectively) with that of bulk undercooled samples (e.g., samples undercooled by $\Delta T > 180$ K, 78 K $< \Delta T <$ 150 K, and $\Delta T < 70$ K, respectively) reveals a surprising similarity, thus indicating similar condition during the solidification processes.

2. Complete massive transformation, which occurs in the immediate vicinity of the chill zone, can not take place in gas-atomization and bulk undercooled solidification, because of the insufficient undercooling achieved before nucleation.

3. Recalescence, which plays an important role in grain refinement in bulk undercooled solidification, are not effective any more in rapid quenching. Consequently, grain refinements occurring in rapid quenching are attributed to different source from that in bulk undercooled solidification.

4. It is the effect of thermal gradient that predominantly controls the crystallization, recalescence and solidification in both rapid quenching and bulk undercooled solidification.


## Acknowledgements

The authors are grateful to the financial support of the Natural Science Foundation of China (Grant NO. 59871041) and the Aeronautical Science Foundation of China (Grant NO. 98H53093).


## References


1. M. C. FLEMINGS, "Solidification Processing" (McGraw-Hill, NY, 1974).
2. S. ANNAVARAPU and D. D. DOHERTY, *Int. J. Powder Metallurgy* **29**(4) (1993) 331.
3. W. KURZ and R. TRIVEDI, *Acta Metall.* **38** (1990) 1.
4. F. DUFLOS and J. F. STOHR, *J. Mater. Sci.* **17** (1992) 3641.
5. Z. Y. JIAN, G. C. YANG and Y. H. ZHOU, *Progress in Natural Science (China)* **7** (1997) 235.
6. D. L. LI, G. C. YANG and Y. H. ZHOU, *J. Mater. Sci.* **30** (1995) 3909.
7. D. M. HERLACH, B. FEUERBACHER and E. SCHLEIP, *Mater. Sci. Eng.* **A133** (1991) 790.
8. T. Z. KATTAMIS, *J. Crystal Growth* **34** (1976) 215.
9. F. LIU, X. F. GUO and G. C. YANG, *J. Mater. Sci.*, accepted.
10. F. LIU, Y. CAI, X. F. GUO and G. C. YANG, *Mater. Sci. Eng.*, Accepted.
11. J. F. LI, G. C. YANG and Y. H. ZHOU, *Mater. Res. Bull.* **33** (1998) 141.
12. W. DU, Ph.D. thesis, Northwestern Polytechnical University, 1998.
13. S. CHAKRAVORTY and D. R. F. WEST, *J. Mater. Sci.* **19** (1984) 3574.
14. E. S. MACHLIN and J. SHAO, *Metall. Trans.* **9A** (1978) 561.
15. B. LUX, *Metal.* **35** (1981) 1235.
16. M. GELL *et al.*, (ed.), "Superalloy" (ASM, 1984).
17. M. BARTH, B. WEI, D. M. HERLACH and B. FEUERBACHER, *Mater. Sci. Eng.* **A178** (1994) 305.
18. E. A. BRANDES (ed.), "Smithells Metalls Reference Book," 6th ed. (Butterworth, Bodmin, 1983).
19. W. J. BOETTINGER, S. R. CORIELL, R. TRIVEDI, in "Rapid Solidification Processing: Principles and Technologies IV," edited by R. Mehrabian P. A. Parrish (Claitor's, Baton Rouge, LA, 1988) p. 13.
20. M. J. AZIZ, *Metall. Mater. Trans.* **27A** (1996) 671.
21. J. LIPTON, W. KURZ and R. TRIVEDI, *Acta Metall. Mater.* **35**(4) (1987) 957
22. J. F. LI, Y. C. LIU, Y. L. LU, G. C. YANG and Y. H. ZHOU, *J. Crystal growth* **192** (1998) 462.
23. T. P. PICCONE, Y. WU, Y. SHIOHARA and M. C. FLEMINGS, *Metall. Trans.* **18A** (1987) 925.
24. L. NASTAC and D. M. STEFANESCU, *ibid.* **27A** (1996) 4675.
25. P. DESNAIN, Y. FAUTRELLE, J. L. MEYER, J. P. RIQUET and F. DURAND, *Acta Metall. Mater.* **38**(8) (1990) 1513.
26. N. MATAN, H. M. A. WINAND, P. CARTER, M. KARUNARATNE, P. D. BOGDANOFF and R. C. REED, *ibid.* **46**(13) (1998) 4587.
27. S. D. FELICELLI, D. R. POIRIER and J. C. HEINRICH, *Metall. Trans.* **29B** (1998) 847.
28. A. KARMA, *Int. J. Non-Equilibrium Processing* **11** (1998) 201.
29. G. L. F. POWELL, *Trans. Met. Soc. AIME* **245** (1969) 1785.
30. G. L. F. POWELL and L. M. HOGAN, *ibid.* **242** (1968) 2133.
31. R. MEHRABIAN, in 1st Conference on Rapid Solidification Processing, edited by R. Mehrabian, B. H. Kear and M. Cohen (Claitor's, Baton Rouge, LA, 1978) p. 9.
32. S. C. HSU, S. CHAKRAVORY and R. MEHRABIAN, *Met. Trans.* **9B** (1978) 1376.
33. L. KUBICAR, S. ADAMISOVA, P. DUHAJ and D. JANICKOVIC, *Mater. Sci. Eng.* **A173** (1993) 367.
34. C. G. LEVI and R. MEHRABIAN, *Metall. Trans.* **13A** (1982) 221.



*Received 15 August 2000*
*and accepted 12 February 2001*